A Step-Wise Approach for Dual Nanoparticle Patterning via Block Copolymer Self-Assembly

Andriy Horechyy, Bhanu Nandan,* Nikolaos E. Zafeiropoulos, Petr Formanek, Ulrich Oertel, Nadja C. Bigall, Alexander Eychmüller, and Manfred Stamm**

A novel step-wise approach for fabrication of periodic arrays of two different types of nanoparticles (NPs), selectively localized at different block copolymer phases is demonstrated. In the first step, pre-synthesized ≈12 nm silver nanoparticles (AgNPs), stabilized with thiol-terminated polystyrene, are mixed with poly(styrene-*block*-vinylpyridine) (PS-*b*-PVP) block copolymer in a common solvent. After film casting and consequent solvent vapor annealing the AgNPs are selectively localized within the PS phase of the block copolymer matrix due to the interaction with PS shell of the nanoparticles. In the second step, ≈2–5 nm gold, platinum, or palladium nanoparticles are directly deposited from their aqueous dispersion on the PVP domains of the self-assembled block copolymer thin films. In such a way, thin films of nanostructured block copolymer with two types of nanoparticles, separated by the two distinct block copolymer phases, are prepared in a step-wise manner. The presented method is very simple and can be applied for various combinations of pre-synthesized nanoparticles where the characteristics of either type of nanoparticles are tuned accordingly in advance, which is more difficult to achieve for in situ synthesized nanoparticles.

1. Introduction

Tremendous interest towards nanomaterials, such as metal or semiconductor nanoparticles (NP), quantum dots (QD), fullerenes, carbon nanotubes (CNT), etc., has come up because of their unique properties, which differ significantly from their bulk analogues and often display size and shape dependency.[1–5] During the past decade significant progress has been made in the improvement of existing and the development of new synthetic methods and strategies which allow to precisely control the composition, structure, size, shape and surface functionality of most of materials produced in the nanometer scale.[5–12] Thus, encouraged by the continuous trend in minimization of devices used in modern high-tech industries and precise tuning of materials properties, nanomaterials are more and more being used as working elements in the design of chemical and biological sensors, energy storage and convertors, catalytic systems, optical devices and others.[1,2,13–15]

Since for many applications precise control over the spatial organization of nanomaterials as device building components is of crucial importance, much attention has been focused on the development of methods to organize them into ordered one-, two- or three-dimensional structures. Among the various strategies used for this purpose, the bottom-up methods have been recognized as an elegant and powerful approach due to their efficiency and high-throughput.[16,17] In particular, block copolymers (BCP) represent one of the most promising self-assembling systems because of the variety of morphologies available whose length scale and periodicity can easily be tailored.[18,19] Owing to this, BCP are widely used for the fabrication of functional nanocomposites containing metal, metal oxide nanoparticles, quantum dots or nanorods.[20–24]

A number of experimental methods have been developed for the incorporation of either pre-synthesized nanoparticles[24–35] or those generated in situ from appropriate precursors[36–40] selectively inside one of the BCP microdomains. Additionally, various techniques have been used for the incorporation of nanomaterials, such as blending of NPs with BCP,[24–26] selective adsorption,[31,32,39] vapor-[41] or electrodeposition.[42] Together with theoretical studies done on such systems[43–45] the binary NP/BCP nanocomposites are now well understood.

In contrast, incorporation of two types of nanoadditives possessing different functional properties (e.g., optical and magnetic) within different domains of the BCP matrix is still a challenge. Some attempts have been made in the past on fabrication of such ternary NP1/NP2/BCP nanocomposites.[46–51] For

Dr. A. Horechyy, Dr. P. Formanek, Dr. U. Oertel, Prof. M. Stamm
Leibniz-Institut für Polymerforschung Dresden e.V. Hohe Straße 6, 01069 Dresden, Germany
E-mail: horechyy@ipfdd.de; stamm@ipfdd.de
Dr. B. Nandan
Department of Textile Technology
Indian Institute of Technology Delhi
New Delhi 110016, India
E-mail: nandan@textile.iitd.ac.in
Prof. N. E. Zaferopoulos
Department of Material Science and Engineering
University of Ioannina
Ioannina 45110, Greece
Dr. N. C. Bigall, Prof. A. Eychmüller
Physical Chemistry
Technical University of Dresden
Bergstraße 66b, 01062 Dresden, Germany

DOI: 10.1002/adfm.201201452

example, utilizing the different chemical nature of the nanoparticle stabilizing shell, pre-synthesized hydrophilic CdSe QDs and hydrophobic gold NPs were selectively sequestered within poly(4-vinylpyridine) (P4VP) and polystyrene (PS) domains of the poly(styrene-*block*-4-vinylpyridine) (PS-*b*-P4VP) BCP.[46] Alternatively, the entropically driven organization of different in size silica and gold nanoparticles within self assembled poly(styrene-*block*-ethylene propylene) matrix was reported by Bockstaller and co-workers.[47]

Undoubtedly, direct mixing of BCPs with pre-synthesized NPs represents the simplest way towards NP/BCP composites. However, this method becomes less attractive for the fabrication of composites highly loaded with nanoparticles mainly due to enhanced tendency of NPs to macrophase segregation and cluster formation.[52] In addition, the morphology of the BCP might be significantly altered by the presence of nanoadditives at concentrations above a certain critical value.[35] For example, using discontinuous molecular dynamic simulations, Schultz and co-workers showed that with an increase in the particle loading, the phase transitions occur from the lamellar to perforated lamellar, cylindrical or disordered morphologies, depending on the particle size, volume fraction and strength of the particle-segment interaction.[43] More recently, Chen and Ruckenstein employed the dissipative particle dynamic simulations for modeling the binary NP/BCP[45] and ternary NP1/NP2/BCP systems,[53] pointing out the importance of considering the whole spectrum of interactions (i.e., particle-particle, particle-segment and segment-segment interactions) in order to predict the morphology and possible phase transitions of such systems.

To overcome the difficulties associated with NPs clustering and morphological perturbations, alternative strategies for the fabrication of ternary NP1/NP2/BCP composites have been developed. Hence, Char and co-workers explored the topographical texture of poly(styrene-*block*-methyl methacrylate) thin films to control the nanoparticle location.[48] The ability of amphiphilic BCP to aggregate into micellar structures has also been used to prepare ternary NP1/NP2/BCP nanocomposites. Such synthetic protocols often involve in situ methods for the particle generation or either a combination of in situ and ex situ methods for loading of different types of NPs. For example, in situ formed iron (III) oxide and pre-synthesized gold nanoparticles were selectively localized in P4VP cores and PS coronas of PS-*b*-P4VP thin film, respectively.[49] Following a similar idea, selective localization of silver and gold nanoparticles within P4VP core and PS corona of PS-*b*-P4VP micelles was demonstrated by Acharya et al.[50] Recently, Russell and co-workers also implemented a micellar route for the fabrication of Pt/Au concentric nanostructures starting from poly(styrene-*block*-2-vinylpyridine-*block*-ethyleneoxide) *tri*-BCP.[51]

Despite the high efficiency of the in situ approaches the reaction conditions prevailing during the synthesis of nanoparticles inside the BCP are not always optimal for achieving the desired properties. Herein, we report on a novel step-wise approach for the selective incorporation of two types of pre-synthesized nanoparticles to different domains of a phase-separated BCP matrix by utilizing a combination of two strategies for nanoparticle incorporation. During the first step, the PS-*b*-PVP BCP is mixed with primary polystyrene-stabilized silver nanoparticles (AgNP, NP1) and deposited as thin films. After subsequent solvent annealing, the AgNPs are preferentially localized in polystyrene phase due to the presence of a compatibilizing PS shell on their surface. In the next step, citrate-stabilized secondary nanoparticles (NP2) (Au, Pt or Pd) are selectively adsorbed onto the PVP domains from their aqueous dispersions, leading to ternary NP1/NP2/BCP composite thin films with each type of NPs selectively located at different BCP domains.

The key advantage of the presented approach is that by partition of the nanoparticle incorporation steps into two distinct procedures morphological disturbances associated with particle aggregation effects are minimized. Moreover, this method becomes more attractive if the application aspects of such ternary composites directly rely on size- or shape-dependent properties of patterned nanomaterials which are more difficult to control when the particles are generated in situ.

2. Results and Discussion

In the present work a step-wise approach was used for the fabrication of ternary NP1/NP2/BCP nanocomposite films as shown in **Scheme 1**. In the first step, the block copolymer and the pre-synthesized primary-type nanoparticles (NP1) were mixed in a common solvent and deposited onto the substrate to form a thin NP1/BCP composite film followed by solvent vapor annealing. Afterwards, the substrate-supported NP1/BCP composite thin films were immersed into an aqueous dispersion of the

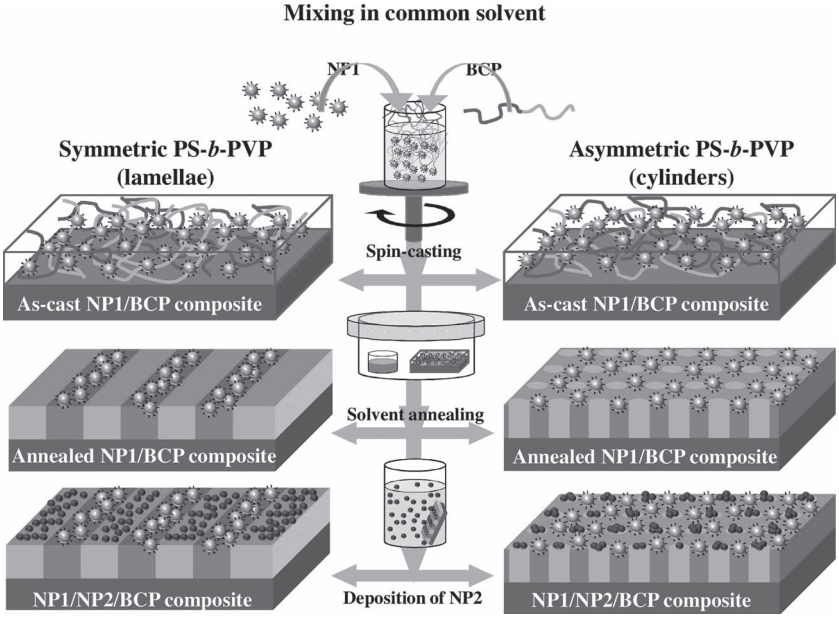

Scheme 1. Schematic illustration of the step-wise approach used for patterning of two types of pre-synthesized nanoparticles exploiting block copolymer self-assembly.

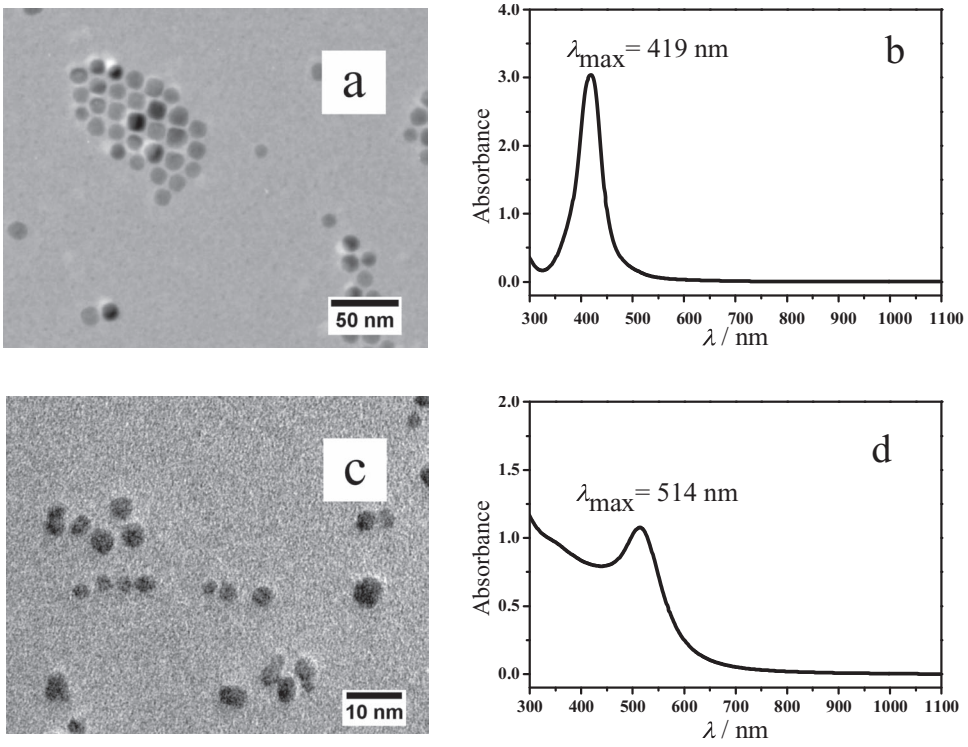

Figure 1. a,c) TEM images of a) AgNPs and c) AuNPs. b,d) UV-vis spectra of b) PS-stabilized AgNPs dispersed in THF and d) citrate-stabilized AuNPs dispersed in water.

secondary nanoparticles (NP2) leading to the formation of ternary NP1/NP2/BCP composites. The presented method involves each type of nanoparticles having been prepared in advance using well-established synthetic procedures. Thus, it gives the advantage to control the nanoparticle characteristics, like for example their optical properties, through the control of particle size, shape and size distribution which that is rather difficult to achieve when the nanoparticles are generated in situ.[40]

Symmetric lamellae-forming poly(styrene-*block*-2-vinylpyridine) and asymmetric cylinder-forming poly(styrene-*block*-4-vinylpyridine) block copolymers (denoted as PS_{50}-*b*-$P2VP_{50}$ and PS_{57}-*b*-$P4VP_{18}$, respectively) were used as polymer matrices for the fabrication of ternary NP1/NP2/BCP composites (for the morphology of neat BCP thin films see the Supporting Information, Figure S1).

The use of PS-containing block copolymers required the primary NP1 to be compatible with the polystyrene phase and non-compatible (or non-miscible) with the complementary phase (i.e., PVP). Such selectivity might be achieved, for example by covering the surface of NP1 with a polymer shell of the same nature as the host block. For example, Kramer and co-workers demonstrated that gold nanoparticles are enthalpically driven selectively to the PS microdomains of a self-assembled PS-*b*-P2VP matrix if their surface is modified with a polystyrene shell.[27,28]

In the present work attention has been focused on the fabrication of composites containing silver nanoparticles (AgNP) which are of particular interest due to their optical properties. Similarly to gold, silver NPs can be modified with polymer ligands using simple and straightforward thiol chemistry. Hence, PS-modified AgNPs were prepared from silver acetate precursor via two reaction steps based on a modified synthetic procedure reported by Hiramatsu and co-workers.[54] The oleylamine used during the first step of AgNP synthesis simultaneously serves the function of both reducing and stabilizing agent but due to the relatively weak interaction between the amino-groups and the silver surface it can be efficiently replaced by various thiol-containing molecules including thiol-terminated polymers. Subsequently, the obtained oleylamine-capped AgNPs were subjected to a ligand-exchange reaction carried out with an excess of thiol-terminated polystyrene (PSSH).

TEM investigations of prepared AgNPs reveal formation of nanoparticles with average size of 12.8 ± 1.1 nm (**Figure 1**a), whereas UV-vis spectrum of PS-modified AgNPs dispersed in THF possess well defined and nearly symmetric surface plasmon resonance (SPR) absorbance peak with its maximum at 419 nm (Figure 1b). FTIR and TGA analyses confirmed the presence of a polystyrene shell on the AgNPs surface, suggesting also complete replacement of oleylamine after the ligand exchange step (Figure S2a–c in the Supporting Information).

The calculated polymer grafting density resulted in the value of 2.2 chains nm^{-2} based on TEM and TGA data. The formation of a densely grafted polymer layer on the nanoparticle surface was considered to be an important requirement to screen possible particle interactions with the PVP chains and achieve their selective segregation to the center of the PS domains of the microphase separated PS-*b*-P2VP BCP matrices.[28] It should be mentioned, that high polymer grafting density is rather difficult to achieve for the planar surfaces via grafting-to methods. Nevertheless, comparable or even higher values were reported

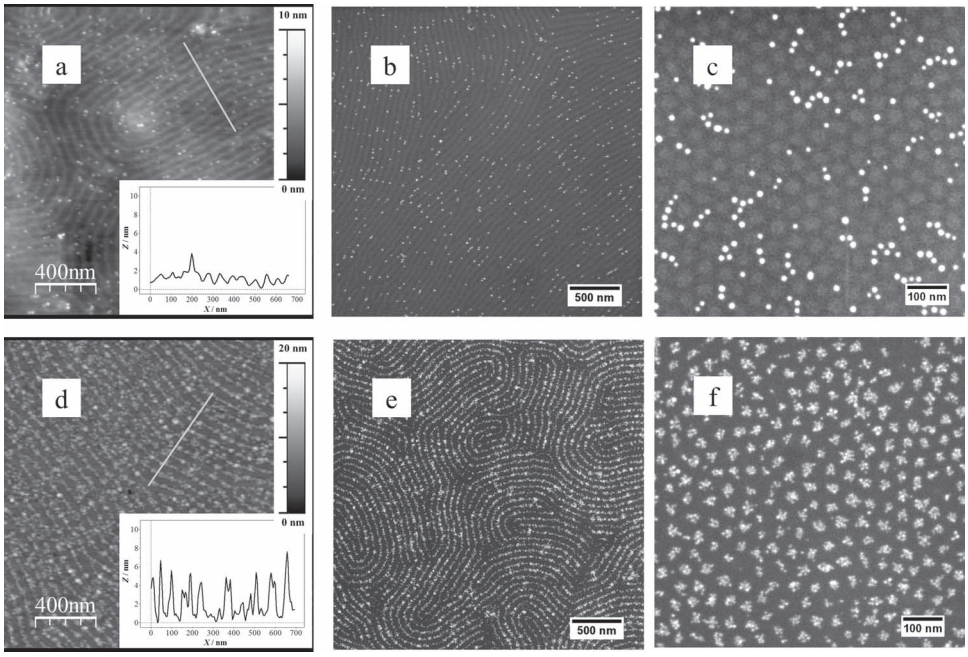

Figure 2. a,b) AFM topography with corresponding cross-sectional profiles (insets) and b,c,e,f) SEM images of a,b) AgNP/PS_{50}-*b*-$P2VP_{50}$, c) AgNP/PS_{57}-*b*-$P4VP_{18}$, d,e) AuNP/PS_{50}-*b*-$P2VP_{50}$, and f) AuNP/PS_{57}-*b*-$P4VP_{18}$ composite thin films.

in literature for polymer-coated gold nanoparticles and attributed to the high apparent curvature of the nanoparticle core and enthalpy gains arising from the Au-S bonds formation counteracting the entropic costs associated with the stretching of the polymer chains.[28,55] The measured separation distances between adjacent AgNPs results in average value of 8.5 ± 3.2 nm, half of which is above estimated RMS end-to-end distance of unperturbed coil (3.3 nm) suggesting thus that tethered PS chains adopt partially stretched conformation (see Figure S2d,e and following text in the Supporting Information).[56]

As secondary nanoparticles (NP2) water-dispersible citrate-stabilized Au, Pt and Pd nanocrystals with 2–5 nm in diameter were used. Recent work done in our group has demonstrated that due to the preferential attraction to the P4VP chains such nanoparticles can be selectively deposited either into P4VP-lined pores of porous PS-*b*-P4VP templates[31] or on the top of the P4VP domains of self-assembled PS-*b*-P4VP BCP.[32] In the present work this method was extended for the fabrication of ternary composites. TEM image and UV-vis spectrum of gold nanoparticles are shown in Figure 1c,d, respectively. For TEM images of Pt and Pd nanoparticles readers are referred to the Supporting Information, Figure S3.

Prior to fabrication of ternary NP1/NP2/BCP composites, the thin BCP films containing only NP1 or NP2 were prepared and examined. **Figure 2**a,b shows topography AFM and SEM images of AgNP/PS_{50}-*b*-$P2VP_{50}$ composite loaded with 2 wt% of silver nanoparticles. Similar to the neat PS_{50}-*b*-$P2VP_{50}$ BCP after solvent vapor annealing a perpendicularly oriented lamellar morphology was observed also for AgNP/PS_{50}-*b*-$P2VP_{50}$ composite thin films. Notably, the AgNPs were found selectively segregated in one of the phase separated BCP microdomains. TEM studies of AgNP/PS_{50}-*b*-$P2VP_{50}$ composites stained with iodine proved that the AgNPs are localized in polystyrene phase (Supporting Information, Figure S4a). With an increase of the AgNPs weight fraction the PS microdomains became progressively loaded with nanoparticles being almost completely filled when the concentration reached 5.0 wt% relative to the BCP fraction. However, when the particle content was further increased, up to 10.0 wt%, the lamellar order and periodicity appeared strongly perturbed by the AgNP presence (Supporting Information, Figure S4b–d). Nevertheless, the alternating character of particle-filled and particle-free regions suggests that even at high loadings AgNPs still remain trapped within the PS phase.

In case of AgNP/PS_{57}-*b*-$P4VP_{18}$ composites, the AgNPs were also found distributed within the major PS phase which forms the matrix, whereas the P4VP domains appeared self-assembled into hexagonally packed cylinders oriented normal to the substrate plane (Figure 2c). It should be mentioned that due to the relatively large AgNP size their inclusions led to a local distortion of the hexagonal arrangement of the P4VP cylinders reflected in an increase of interdomain spacing and appearance of defects.

Figure 2d–f depict SEM images of AuNP/PS_{50}-*b*-$P2VP_{50}$ and AuNP/PS_{57}-*b*-$P4VP_{18}$ composite thin films taken after deposition of the gold nanoparticles. Due to preferential attraction to the PVP chains the AuNPs are selectively deposited atop of either lamellar P2VP or cylindrical P4VP microdomains. Although the proposed approach allows precise control of the primary NP1 concentration, the loading of the secondary NP2 could be coarsely tuned by the exposure time maintained for their deposition. From the comparison of series of SEM images taken after different AuNP deposition times it becomes evident that the BCP film surface appears progressively covered with the nanoparticles with an extension of particles deposition time, approaching the values of 47% for lamellar and 28% for cylindrical morphology after 24 h of exposure. Analysis of SEM

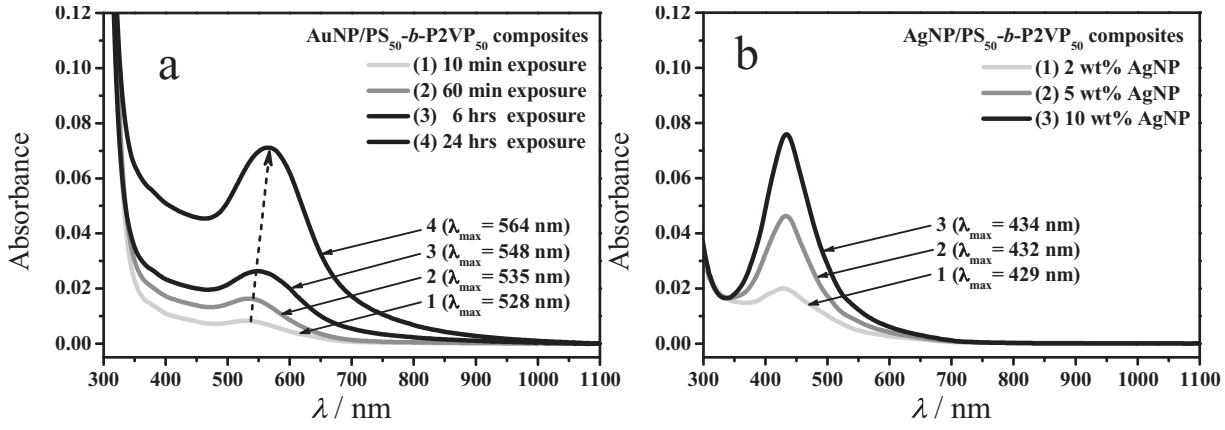

Figure 3. UV-vis spectra of a) AuNP/PS_{50}-*b*-$P2VP_{50}$ composites after different AuNP deposition times and b) AgNP/PS_{50}-*b*-$P2VP_{50}$ composites loaded with different amount of AgNPs.

and AFM images also gives evidence that AuNP start to form clusters whose size becomes progressively larger in both lateral and normal dimensions as particles deposition time increases (for details see Supporting Information, Figure S5,S6).

The UV-vis spectra of series of AuNP/PS_{50}-*b*-$P2VP_{50}$ and AgNP/PS_{50}-*b*-$P2VP_{50}$ composites are shown in **Figure 3**. As can be seen, for AuNP/PS_{50}-*b*-$P2VP_{50}$ composites, the position of the SPR absorbance peak maxima of gold NPs is progressively red-shifted as the particle deposition time increases (Figure 3a). Similar gradual red shift was also found for AuNP/PS_{57}-b-$P4VP_{18}$ composites as the particles deposition time was extended (Supporting Information, Figure S7). Taking into account SEM and AFM results discussed above, observed red shift is attributed to an increased clustering of AuNP along the lamellar P2VP or cylinder-forming P4VP domains as the amount of adsorbed nanoparticles increases with time.[57]

In contrast, for the AgNP/PS_{50}-*b*-$P2VP_{50}$ composites the position of SPR absorbance peak maxima of AgNPs remained almost unchanged for the composites loaded with different amount of AgNPs (Figure 3b). The position of peak maxima remained also unchanged when silver-containing composites (either AgNP/PS_{50}-*b*-$P2VP_{50}$ or AgNP/PS_{57}-*b*-$P4VP_{18}$) were annealed in different solvents and for different period of time. This suggests that, in contrast to gold NP, the AgNPs do not aggregate after solvent vapor annealing.

For preparation of ternary composites, solvent annealed AgNP/PS-*b*-PVP thin films with perpendicularly oriented microdomains were immersed into NP2 aqueous dispersions, allowing the NP2 to selectively adsorb atop of the PVP phase. Considering the results discussed above, for further experiments the concentration of AgNP in BCP was limited to 5.0 wt% in order to preserve the periodic lamellar structure of the AgNP/PS_{50}-*b*-$P2VP_{50}$ composites and prevent the hexagonal order of P4VP cylinder from getting perturbed by AgNP inclusions.

Representative AFM topography images of ternary AgNP/NP2/PS_{50}-*b*-$P2VP_{50}$ composites obtained after exposure of AgNP/PS_{50}-*b*-$P2VP_{50}$ thin films to various NP2 dispersions for 24 h with corresponding cross sectional profiles (insets) taken across the lines on topography images are shown in **Figure 4**. Importantly, after deposition of the NP2 the initial morphology was not disturbed maintaining the perpendicular lamella structure both before and after NP2 deposition. The presence of the NP2 becomes evident from the comparison of topographic AFM images of AgNP/PS_{50}-*b*-$P2VP_{50}$ (Figure 2b), ternary composites (Figure 4) and their corresponding cross sectional profiles.

Although due to increased surface roughness the primary AgNPs became difficult to visualize with AFM imaging after deposition of the secondary NP2, the presence of both AgNP and AuNP is evident from the UV-vis spectra of ternary AgNP/

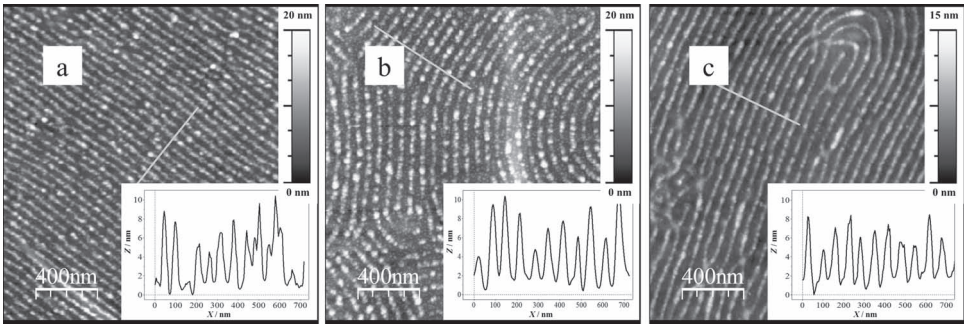

Figure 4. AFM topography images with corresponding cross-sectional profiles (insets) of a) AgNP/AuNP/PS_{50}-*b*-$P2VP_{50}$, b) AgNP/PtNP/PS_{50}-*b*-$P2VP_{50}$, and c) AgNP/PdNP/PS_{50}-*b*-$P2VP_{50}$ ternary composites taken after 24 h of NP2 deposition.

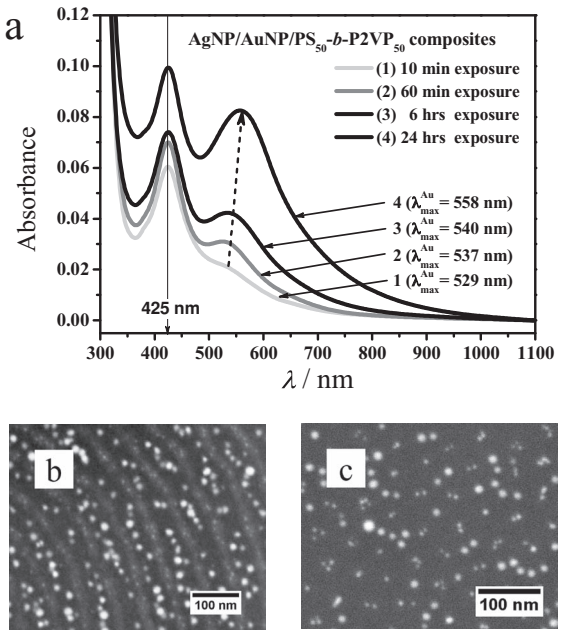

Figure 5. a) UV-vis spectra of ternary AgNP/AuNP/PS_{50}-*b*-$P2VP_{50}$ composites measured after different time of AuNP deposition. The concentration of the AgNPs in all samples was kept 5.0 wt%. SEM images of b) lamellar AgNP/AuNP/PS_{50}-*b*-$P2VP_{50}$ and c) cylindrical AgNP/AuNP/PS_{57}-*b*-$P4VP_{18}$ composites, respectively.

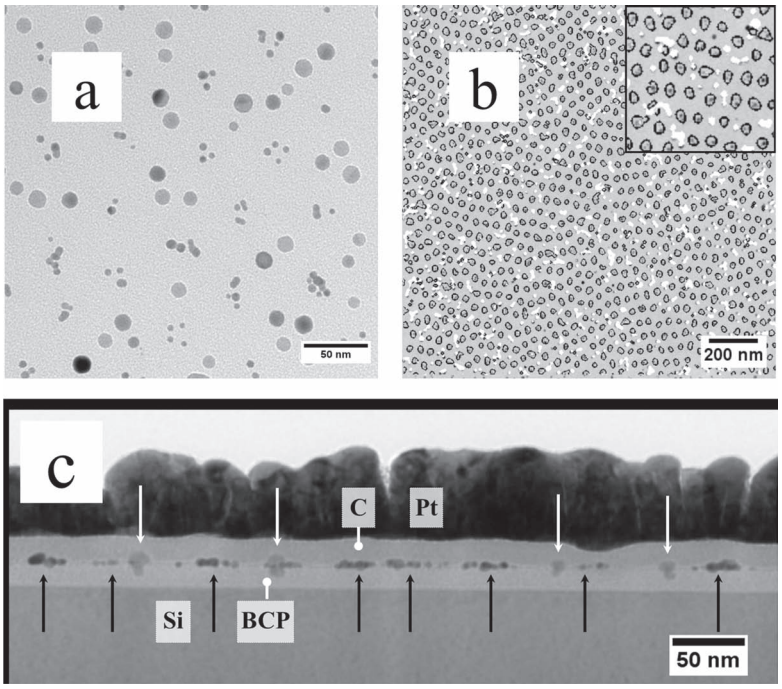

Figure 6. a) High-magnification TEM image of the ternary AuNP/AgNP/PS_{57}-*b*-$P4VP_{18}$ composite thin film depicting the presence of larger AgNPs and smaller AuNPs. b) The overlay of the TEM image of the ternary AuNP/AgNP/PS_{57}-*b*-$P4VP_{18}$ with the contours corresponding to the presence of nitrogen (the P4VP phase, black unfilled contours) and AgNPs (white spots). The contours are based on the elemental maps determined form the energy filtered TEM images. The loading of the AgNP was 5.0 wt% and the deposition time of the AuNP was 1 h. Inset in (b) is a magnified part of the image. c) Cross-sectional TEM image of FIB lamella of the ternary AuNP/AgNP/PS_{57}-*b*-$P4VP_{18}$ composite. Black and white arrows depict positions of smaller AuNPs atop of P4VP microdomains and larger AgNPs, respectively.

AuNP/PS_{50}-*b*-$P2VP_{50}$ composites (**Figure 5**a). Two SPR absorbance peaks are detectable for the composites loaded with both silver and gold NPs, in contrast to a single SPR peak observed for the composites containing either AgNPs or AuNPs (Figure 3). Due to the nanoparticles clustering the position of the SPR peak maxima of gold underwent a gradual red shift (similar to AuNP/PS_{50}-*b*-$P2VP_{50}$) as the particle deposition time was increased. In contrast absorbance peak of silver is slightly blue-shifted, which is probably due to an overlap of SPR peaks of silver and gold.

It is important to mention that due to the difference in size between the AgNPs (12.8 nm) and the Au (Pt, Pd) nanocrystals (2–5 nm) the presence and exact position of either type of NPs was possible to detect with conventional SEM. From the SEM image shown in Figure 5b it is evident that both the larger AgNPs and the smaller PdNPs are selectively localized within alternating perpendicular lamellae, consisting of PS and P2VP, respectively. Similarly, the presence of both larger AgNPs and smaller AuNPs can be resolved in the SEM image of AgNP/AuNP/PS_{57}-*b*-$P4VP_{18}$ composite (Figure 5c), as also proved by the UV-vis experiments (Supporting Information, Figure S7).

A bright field TEM image of the ternary AgNP/AuNP/PS_{57}-*b*-$P4VP_{18}$ composite is shown in **Figure 6**a. Due to the presence of AgNP inclusions it is rather difficult to visualize the actual positions of the AuNPs within the BCP matrix. Nevertheless, their quasi-hexagonal arrangement can be seen in Figure 6b which is an overlay of the bright field TEM image elemental maps derived form the energy-filtered TEM images, where the presence of nitrogen (i.e., the P4VP domains) is marked with the black contours and the AgNPs are marked with the white spots (see Supporting Information for details).

The distribution of nanoparticles through the film thickness can be validated from the cross-sectional TEM image of AgNP/AuNP/PS_{57}-*b*-$P4VP_{18}$ composite shown in Figure 6c. As it was expected, the AuNPs being deposited from their aqueous dispersion localize atop of the PVP domains of the BCP thin film (pointed with black arrows). Moreover, the larger PS-stabilized AgNPs were also found localized close to the polymer/air interface (white arrows). Similar tendency of PS-stabilized AgNP to segregate close to the polymer/air interface was also found for composites having lamellar morphology and can be explained as a consequence of relatively large AgNPs size and presence of the densely grafted polymer layer on their surface.[56]

3. Conclusions

This work presents a novel step-wise approach for the fabrication of ternary NP1/NP2/BCP composites having either type of nanoparticles selectively localized within a particular microdomain of phase separated block copolymer films. Within this method, both types of NPs were prepared in advance using well established synthetic methods allowing thus the precise control over their main

characteristics, such as composition, size, shape or polydispersity, which can not easily be controlled when the nanoparticles are generated in situ within the BCP matrix. This is of pivotal importance if the application aspects of such ternary composites require consideration of the inherent properties of both NPs, often being size- and shape-dependent, and those being related to the particles collective behavior which depends on their spatial organization. Although AgNP inclusions within the PS matrix led to a distortion of the hexagonal order of neighboring P4VP cylinders, the problem might be overcome using the nanoparticles with sufficiently small size. The partition of the particle incorporation procedures in two distinct steps, that is direct mixing of NP1 with BCP, followed by deposition of NP2 onto the pre-formed NP1/BCP template, allows to effectively load either type of pre-synthesized NPs overcoming in such a way the difficulties associated with nanoparticle agglomeration and macrophase separation, often observed at high nanoparticle fraction. The proposed method is applicable for various combinations of nanoparticles and represents a simple and straightforward route towards composite materials with multiple functionalities.

4. Experimental Section

Materials: Thiol-functionalized polystyrene (PSSH, M_n = 5300 g mol^{-1}, PDI = 1.10), block copolymers poly(styrene-*block*-2-vinylpyridine) (PS_{50}-*b*-$P2VP_{50}$, M_n(PS) = 50.0 kg mol^{-1}, M_n(P2VP) = 50.0 kg mol^{-1}, PDI = 1.16) and poly(styrene-*block*-4-vinylpyridine) (PS_{57}-*b*-$P4VP_{18}$, M_n(PS) = 57.5 kg mol^{-1}, M_n(P4VP) = 18.5 kg mol^{-1}, PDI = 1.14) were purchased from Polymer Source, Inc., Canada and used as received. Silver acetate (CH_3COOAg, 99%), sodium tetrachloroaureate ($NaAuCl_4$, 99.9%), chloroplatinic acid (H_2PtCl_6, ACS reagent), palladium (II) chloride ($PdCl_2$, 99.999%), sodium citrate (99%), sodium borohydride ($NaBH_4$, 96%) and oleylamine (70%) were purchased from Sigma Aldrich and used as received. Toluene, 1,4-dioxane, THF, ethanol, 1,4-dichlorobenzene, dichloromethane, purchased from Acros Organics, were of analytical grade and used without any purification. Hydrochloric acid (36%), hydrogen peroxide (30%) (Merck) and ammonium hydroxide solution (28%) (Acros) and were of analytical grade and used as received. Highly polished single-crystal silicon wafers ({100} orientation) with ≈1.5 nm native silicon oxide layer (Semiconductor Processing Co) and ≈1-mm-thick glass substrates were used as substrates for thin film deposition.

Synthesis of Polystyrene-Coated Silver Nanoparticles: Polystyrene-coated silver nanoparticles (AgNP) 12.8 ± 1.1 nm in size were prepared in two steps using a modified synthetic procedure reported by Hiramatsu and Osterloh.[54] During the first step oleylamine stabilized AgNPs were synthesized under reflux in 1,2-dichlorobenzene starting from silver acetate as metal precursor. Next, a ligand-exchange step was performed to replace oleylamine with thiol-terminated polystyrene. More details on the synthetic conditions, post-treatment and purification steps can be found in the Supporting Information.

Synthesis of Citrate Stabilized Noble Metal Nanoparticles (AuNPs, PtNPs, PdNPs): Water soluble Au, Pt and Pd nanoparticles with average diameter of 3.5 ± 0.5, 2.5 ± 0.5, and 3.8 ± 0.5 nm, respectively, were prepared using procedures similar to the synthetic route described by Brown et al.[58] The precursors used for the preparation of the gold and platinum NPs were aqueous solutions of sodium tetrachloroaureate ($NaAuCl_4$) and chloroplatinic acid (H_2PtCl_6), whilst hydrogen tetrachloropalladate (the precursor for the PdNP) was obtained by dissolving palladium (II) chloride in hydrochloric acid in the molar ratio $PdCl_2$:HCl 1:2. Aqueous dispersions of as-synthesized citrate-stabilized noble metal NPs were used for further experiments. More details on the synthetic procedures used for the syntheses of citrate-stabilized metal NPs can be found in the Supporting Information.

Preparation of AgNPs/BCP Composites: Stock solutions of PS-modified AgNPs and PS-*b*-PVP BCP were prepared in THF and mixed together to yield nanoparticle concentrations ranging from 0.0 to 10.0 wt% with respect to the PS-*b*-PVP content. The BCP concentration was adjusted to 0.5–1.0 wt% by the addition of THF. The AgNPs/BCP composites in THF were stirred at room temperature for 24 h to ensure homogenous mixing of the nanoparticles and the BCP. Before the film deposition the THF solutions of PS-*b*-PVP BCPs and AgNPs/BCP composites were filtered through a 0.2 µm PTFE membrane filter to remove possible particulate species.

Thin Film Preparation and Annealing: Silicon and glass wafers were pre-cleaned by repeated sonication in CH_2Cl_2 followed by treatment with a mixture of water, aqueous solutions of hydrogen peroxide (30%) and ammonium hydroxide (28%) (4:1:1 by volume) for 1 h at 80 °C. The wafers were thoroughly rinsed with Milli-Q water and dried with nitrogen flow before being used as substrates for thin film deposition. The 20–30 nm thin films were deposited onto pre-cleaned wafers by spin- or dip-coating from the BCP or AgNPs/BCP composite solutions. The film thickness was adjusted via tuning the block copolymer concentration and the rotation/withdrawing speed during thin film preparation. The solvent vapor annealing of the thin films was performed in a glass chamber saturated with 1,4-dioxane vapor for 10–180 min.

Deposition of Au, Pt and Pd Nanoparticles: Si and glass substrates with deposited and solvent annealed PS-*b*-PVP and AgNPs/PS-*b*-PVP composite films were dipped into aqueous dispersions of Au, Pt or Pd nanoparticles for different period of time (i.e., from 10 min to 24 h), washed repeatedly with de-ionized water to remove non-adsorbed or weakly-adsorbed nanoparticles and dried with nitrogen flow.

Characterization: Atomic force microscopy (AFM) imaging was performed in the tapping mode (Dimension 3100 SFM, Digital Instruments, Inc., Santa Barbara, CA) using silicon cantilevers with resonance frequency of 60–70 kHz and a tip radius of ≈10 nm. Scanning electron microscopy was performed using a NEON 40 FIB-SEM workstation (Carl Zeiss AG, Germany) operated at 3 kV. In order to resolve the nanoparticle positions within the BCP matrix thin films of NP/BCP composites supported on Si substrates were studied with SEM without any metal sputtered atop of the films. A Libra200 transmission electron microscope with integrated Ω-type energy filter (Carl Zeiss AG, Germany) operated at 200 kV was used to perform TEM imaging. NP specimens for TEM investigations were prepared by drying a droplet of nanoparticles dispersions in THF (in case of AgNP) or in water (in case of Au, Pt or Pd nanoparticles) on amorphous carbon coated copper grids (200-mesh, Plano GmbH, Wetzlar, Germany). The number-average size and size distribution of the NPs were estimated by measuring the size of at least 300 individual particles using the ImageJ software. For TEM investigations, the NP/BCP composite thin films were etched from Si wafers by immersion into a 1M NaOH water solution and transferred onto 400-mesh copper grid. FTIR spectra were recorded with a Vertex 80v spectrometer (Bruker, Germany) in the transmission mode (KBr technique). TGA measurements were performed on a TA Q5000 thermal analyzer (TA instruments, USA) at a heating rate of 10 K/min in a nitrogen atmosphere. The UV-vis spectra of the AgNPs and AuNPs dispersions were recorded in transmission mode using a Lambda 900 Perkin-Elmer spectrophotometer, whereas the spectra of the NP/BCP composite thin films were measured with a Cary 6000i (Varian) instrument in the wavelength range λ = 300–1100 nm (averaging time 0.3 s, spectral bandwidth 1 nm). Lamella for cross-sectional TEM imaging was prepared using NEON 40 FIB-SEM workstation (Carl Zeiss AG, Germany) equipped with a Ga ion beam and operated at 30 kV. The samples were initially covered with 15-nm-thick carbon layer to provide contrast for visualization of nanoparticles and then sputtered with 40-nm-thick platinum layer. Finally, a localized additional 15-nm-thick platinum layer was deposited with the ion beam over the area selected for lamella preparation. The samples were milled and polished with the FIB to give a 100-nm-thick lamella.

Supporting Information

Supporting information is available from the Wiley Online Library or from the author.

Acknowledgements

The authors thank Mrs. L. Häussler and G. Adam (IPF Dresden) for the TGA and FTIR experiments, and also Mr. M. Göbel for preparation of FIB lamellae. The research was supported by the priority program of the Deutsche Forshungsgemeinschaft (SPP1165, Project No. STA324/31).

Received: May 30, 2012
Published online: September 12, 2012

[1] T. Trindade, P. O'Brien, N. L. Pickett, *Chem. Mater.* **2001**, *13*, 3843.
[2] P. K. Jain, X. H. Huang, I. H. El-Sayed, M. A. El-Sayed, *Acc. Chem. Res.* **2008**, *41*, 1578.
[3] P. Moriarty, *Rep. Prog. Phys.* **2001**, *64*, 297.
[4] A. Moores, F. Goettmann, *New J. Chem.* **2006**, *30*, 1121.
[5] C. Burda, X. B. Chen, R. Narayanan, M. A. El-Sayed, *Chem. Rev.* **2005**, *105*, 1025.
[6] S. H. Sun, H. Zeng, D. B. Robinson, S. Raoux, P. M. Rice, S. X. Wang, G. X. Li, *J. Am. Chem. Soc.* **2004**, *126*, 279.
[7] J. Park, J. Joo, S. G. Kwon, Y. Jang, T. Hyeon, *Angew. Chem. Int. Ed.* **2007**, *46*, 4630.
[8] A. H. Lu, E. L. Salabas, F. Schuth, *Angew. Chem. Int. Ed.* **2007**, *46*, 1222.
[9] A. R. Tao, S. Habas, P. D. Yang, *Small* **2008**, *4*, 310.
[10] N. A. Frey, S. Peng, K. Cheng, S. H. Sun, *Chem. Soc. Rev.* **2009**, *38*, 2532.
[11] T. K. Sau, A. L. Rogach, *Adv. Mater.* **2010**, *22*, 1781.
[12] R. A. Sperling, W. J. Parak, *Philos. Trans. R. Soc., A* **2010**, *368*, 1333.
[13] A. S. Arico, P. Bruce, B. Scrosati, J. M. Tarascon, W. Van Schalkwijk, *Nat. Mater.* **2005**, *4*, 366.
[14] M. E. Stewart, C. R. Anderton, L. B. Thompson, J. Maria, S. K. Gray, J. A. Rogers, R. G. Nuzzo, *Chem. Rev.* **2008**, *108*, 494.
[15] A. K. Gupta, M. Gupta, *Biomaterials* **2005**, *26*, 3995.
[16] M. Lazzari, C. Rodriguez-Abreu, J. Rivas, M. A. Lopez-Quintela, *J. Nanosci. Nanotechnol.* **2006**, *6*, 892.
[17] M. Grzelczak, J. Vermant, E. M. Furst, L. M. Liz-Marzan, *ACS Nano* **2010**, *4*, 3591.
[18] F. S. Bates, G. H. Fredrickson, *Phys. Today* **1999**, *52*, 32.
[19] I. W. Hamley, *Nanotechnology* **2003**, *14*, R39.
[20] M. R. Bockstaller, R. A. Mickiewicz, E. L. Thomas, *Adv. Mater.* **2005**, *17*, 1331.
[21] A. Haryono, W. H. Binder, *Small* **2006**, *2*, 600.
[22] J. Bang, U. Jeong, D. Y. Ryu, T. P. Russell, C. J. Hawker, *Adv. Mater.* **2009**, *21*, 4769.
[23] E. Ploshnik, A. Salant, U. Banin, R. Shenhar, *Adv. Mater.* **2010**, *22*, 2774.
[24] Y. Lin, A. Boker, J. B. He, K. Sill, H. Q. Xiang, C. Abetz, X. F. Li, J. Wang, T. Emrick, S. Long, Q. Wang, A. Balazs, T. P. Russell, *Nature* **2005**, *434*, 55.
[25] C. Xu, K. Ohno, V. Ladmiral, R. J. Composto, *Polymer* **2008**, *49*, 3568.
[26] A. Horechyy, N. E. Zafeiropoulos, B. Nandan, P. Formanek, F. Simon, A. Kiriy, M. Stamm, *J. Mater. Chem.* **2010**, *20*, 7734.
[27] J. J. Chiu, B. J. Kim, E. J. Kramer, D. J. Pine, *J. Am. Chem. Soc.* **2005**, *127*, 5036.
[28] B. J. Kim, J. Bang, C. J. Hawker, E. J. Kramer, *Macromolecules* **2006**, *39*, 4108.
[29] Y. Zhao, K. Thorkelsson, A. J. Mastroianni, T. Schilling, J. M. Luther, B. J. Rancatore, K. Matsunaga, H. Jinnai, Y. Wu, D. Poulsen, J. M. J. Frechet, A. P. Alivisatos, T. Xu, *Nat. Mater.* **2009**, *8*, 979.
[30] I. Garcia, A. Tercjak, N. E. Zafeiropoulos, M. Stamm, I. Mondragon, *Macromol. Rapid Commun.* **2007**, *28*, 2361.
[31] B. Nandan, E. B. Gowd, N. C. Bigall, A. Eychmuller, P. Formanek, P. Simon, M. Stamm, *Adv. Funct. Mater.* **2009**, *19*, 2805.
[32] E. B. Gowd, B. Nandan, N. C. Bigall, A. Eychmuller, P. Formanek, M. Stamm, *Polymer* **2010**, *51*, 2661.
[33] M. M. A. Kashem, J. Perlich, A. Diethert, W. N. Wang, M. Memesa, J. S. Gutmann, E. Majkova, I. Capek, S. V. Roth, W. Petry, P. Muller-Buschbaum, *Macromolecules* **2009**, *42*, 6202.
[34] Q. F. Li, J. B. He, E. Glogowski, X. F. Li, J. Wang, T. Emrick, T. P. Russell, *Adv. Mater.* **2008**, *20*, 1462.
[35] B. J. Kim, J. J. Chiu, G. R. Yi, D. J. Pine, E. J. Kramer, *Adv. Mater.* **2005**, *17*, 2618.
[36] J. I. Abes, R. E. Cohen, C. A. Ross, *Mater. Sci. Eng., C* **2003**, *23*, 641.
[37] S. Horiuchi, T. Fujita, T. Hayakawa, Y. Nakao, *Langmuir* **2003**, *19*, 2963.
[38] S. H. Yun, B. H. Sohn, J. C. Jung, W. C. Zin, J. K. Lee, O. Song, *Langmuir* **2005**, *21*, 6548.
[39] J. Chai, J. M. Buriak, *ACS Nano* **2008**, *2*, 489.
[40] J. I. Abes, R. E. Cohen, C. A. Ross, *Chem. Mater.* **2003**, *15*, 1125.
[41] S. Park, J. Y. Wang, B. Kim, T. P. Russell, *Nano Lett.* **2008**, *8*, 1667.
[42] O. Seifarth, R. Krenek, I. Tokarev, Y. Burkov, A. Sidorenko, S. Minko, M. Stamm, D. Schmeisser, *Thin Solid Films* **2007**, *515*, 6552.
[43] A. J. Schultz, C. K. Hall, J. Genzer, *Macromolecules* **2005**, *38*, 3007.
[44] A. C. Balazs, T. Emrick, T. P. Russell, *Science* **2006**, *314*, 1107.
[45] H. Y. Chen, E. Ruckenstein, *J. Chem. Phys.* **2009**, *131*.
[46] C. M. Huang, K. H. Wei, *Macromolecules* **2008**, *41*, 6876.
[47] M. R. Bockstaller, Y. Lapetnikov, S. Margel, E. L. Thomas, *J. Am. Chem. Soc.* **2003**, *125*, 5276.
[48] J. G. Son, W. K. Bae, H. M. Kang, P. F. Nealey, K. Char, *ACS Nano* **2009**, *3*, 3927.
[49] B. H. Sohn, J. M. Choi, S. I. Yoo, S. H. Yun, W. C. Zin, J. C. Jung, M. Kanehara, T. Hirata, T. Teranishi, *J. Am. Chem. Soc.* **2003**, *125*, 6368.
[50] H. Acharya, J. Sung, B. H. Sohn, D. H. Kim, K. Tamada, C. Park, *Chem. Mater.* **2009**, *21*, 4248.
[51] H. D. Koh, S. Park, T. P. Russell, *ACS Nano* **2010**, *4*, 1124.
[52] S. W. Yeh, K. H. Wei, Y. S. Sun, U. S. Jeng, K. S. Liang, *Macromolecules* **2005**, *38*, 6559.
[53] H. Y. Chen, E. Ruckenstein, *Polymer* **2010**, *51*, 5869.
[54] H. Hiramatsu, F. E. Osterloh, *Chem. Mater.* **2004**, *16*, 2509.
[55] M. K. Corbierre, N. S. Cameron, R. B. Lennox, *Langmuir* **2004**, *20*, 2867.
[56] P. F. Green, *Soft Matter.* **2011**, *7*, 7914.
[57] L. M. Liz-Marzan, *Langmuir* **2006**, *22*, 32.
[58] K. R. Brown, D. G. Walter, M. J. Natan, *Chem. Mater.* **2000**, *12*, 306.